A generalized self-consistent model for quantum tunneling current in dissimilar metal-insulator-metal junction

View Online   Export Citation   CrossMark

Sneha Banerjee and Peng Zhang[a] (iD)

AFFILIATIONS

Department of Electrical and Computer Engineering, Michigan State University, East Lansing, Michigan 48824-1226, USA

[a] email: pz@egr.msu.edu

ABSTRACT

We study the current density-voltage ($J - V$) characteristics of dissimilar metal-insulator-metal (MIM) nanoscale tunneling junctions using a self-consistent quantum model. The model includes emissions from both cathode and anode, and the effects of image charge potential, space charge and exchange correlation potential. The $J - V$ curves span three regimes: direct tunneling, field emission, and space-charge-limited regime. Unlike similar MIM junctions, the $J - V$ curves are polarity dependent. The forward (higher work function metal is negatively biased) and reverse (higher work function metal is positively biased) bias $J - V$ curves and their crossover behaviors are examined in detail for various regimes, over a wide range of material properties (work function of the electrodes, electron affinity and permittivity of the insulator). It is found that the asymmetry between the current density profiles increases with the work function difference between the electrodes, insulator layer thickness and relative permittivity of the insulator. This asymmetry is profound in the field emission regime and insignificant in the direct tunneling, and space charge limited regimes.

I. INTRODUCTION

Quantum tunneling[1,2] is important to nanoelectronic circuit designs, tunneling electrical contacts,[3] scanning tunneling microscopes (STMs),[4,5] plasmonic resonators,[6–8] carbon nanotubes,[9–13] graphene[14,15] and other two-dimensional (2D) materials based devices[16,17] and novel vacuum nano-devices.[18–21] Quantum tunneling effects impose serious challenges to the physical scaling down of traditional electronic circuits.[22] However, it enables the development of future tunneling field-effect transistors (TFETs), which are envisioned to further extend Moore's law.[23] Tunneling in electrical contacts can be utilized to mitigate current crowding and nonuniform heat deposition in the contact region.[3] Tunneling phenomenon may also introduce new regimes in quantum plasmonics.[24] Hence, it is critical to accurately characterize the current density-voltage ($J - V$) behaviors in nano-scale metal-insulator-metal (MIM) junctions, for a variety of material properties and junction dimensions.

Tunneling effects between electrodes separated by thin insulating films have been studied extensively by Simmons[2,25–28] in

1960s. Although in Simmons' theory the effects of image charge potential are considered, the electron space charge potential and the electron exchange-correlation potential inside the insulator thin films, are ignored. Simmons' model is reliable only in low voltage regime for limited parameter space (insulator gap > 1 nm, barrier height > 3 eV).[24] The effects of space charge in a vacuum nanogap have been studied[29–31] extensively, with extensions to short pulse.[32] Recently, Zhang[24] proposed a self-consistent model (SCM) to characterize quantum tunneling current in similar MIM junctions, considering current flowing from both the electrodes. It is found that the $J - V$ characteristics may be divided into three regimes: direct tunneling, field emission, and space-charge-limited regime.[24]

However, the SCM for similar MIM junctions is not sufficient to characterize electron tunneling through MIM junctions formed between two electrodes with different work functions, where the $J - V$ characteristic is dependent upon the polarity of the bias voltage.[25] The asymmetry of the polarity-dependent $J - V$ behavior is important to harmonic mixers, rectifiers, millimeter wave and

infrared detectors.[33] Several efforts have been made to enhance this asymmetry in dissimilar MIM tunnel diodes.[33–35] The asymmetric $J − V$ characteristics in MIM structure is also of high interest in memory devices such as dynamic random-access memory (DRAM) capacitors[36] or memristors.[37] Additionally, dissimilar MIM junctions are naturally formed between scanning tunneling microscope's tip and substrate[4,5] and in nanoscale electrical contacts.[3]

In this paper, we extend the theory of Zhang[24] to dissimilar MIM junctions (Figure 1). Following Simmons,[25] we define the forward bias (FB) and reverse bias (RB) of the MIM junction, when the metal electrode with higher work function is negatively and positively biased, respectively. We provide a detailed study of FB and RB asymmetry and its dependence on a wide range of input parameters (work functions of the electrodes, thickness and relative permittivity of the insulator), for different voltage regimes. The FB and RB characteristics are found to cross over at high voltages in the field emission regime. The asymmetry between the current density profiles increases with the work function difference of the electrodes, the thickness or permittivity of the insulator layer. The strong saturation of tunneling current density in the space charge limited (SCL) regime, which can be achieved under ultrafast pulsed excitation,[38] is explored for different input parameters.
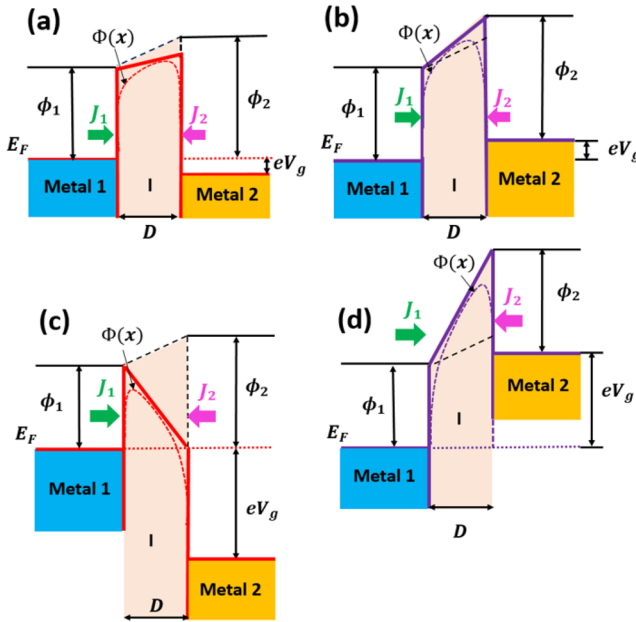

FIG. 1. Dissimilar metal-insulator-metal (MIM) tunneling junction. The metal electrodes have equilibrium Fermi level E_F and work function W_1 and W_2 (in these schematics we assume $W_2 > W_1$). $\phi_1 = W_1 − X$, $\phi_2 = W_2 − X$, where X is electron affinity of the insulator. The insulator thin film thickness is D. The applied voltage bias is V_g. The current densities emitted from the electrode 1 and 2 into the gap are J_1 and J_2, respectively. (a), (c) reverse bias (W_2 is positively biased) condition; (b), (d) forward bias (W_2 is negatively biased) condition. (a), (b) represent low and (c), (d) represent high bias voltage conditions.

II. FORMULATION

Our self-consistent model (SCM) formulation is based on the formulation of similar MIM junctions.[24] The potential barrier formed between the two electrodes is,

$$\Phi(x) = E_F + \Phi_w(x) + \Phi_{image}(x) + eV(x) + \Phi_{xc}(x), \quad (1)$$

where E_F is the equilibrium Fermi level; $\Phi_w(x) = \phi_1 + (\phi_2 − \phi_1)x/D$; $\phi_1 = W_1 − X$, $\phi_2 = W_2 − X$; W_1 and W_2 are the work functions of metal electrode 1 and 2 respectively; X is electron affinity of the insulator; $\Phi_{image}(x) = \left(−e^2/8\pi\epsilon_r\epsilon_0\right)\left[1/2x + \sum_{n=1}^{\infty}\left(nD/(n^2D^2 − x^2)\right) − 1/nD\right)\right]$ is the image charge potential energy including the effect of anode screening,[31] where e is the electron charge, ϵ_0 is the permittivity of free space, ϵ_r is the relative permittivity of the insulator, and D is the gap distance; the electric potential $eV(x) = eV_g x/D + eV_{sc}(x)$, where the two terms are the potential due to the external applied voltage V_g and the potential due to the electron space charge, respectively; and $\Phi_{xc}(x) = \left(\epsilon_{xc} − (r_s/3)d\epsilon_{xc}/dr_s\right) \times E_H$ is the electron exchange-correlation potential calculated by the Kohn-Sham local density approximation (LDA),[39] where $r_s(x)$ is the local Seitz radius $\left[4\pi n(x)(r_s a_0)^3/3 = 1\right]$ in terms of the Bohr radius a_0 = 0.0529 nm, $n(x)$ is the electron density, E_H = 27.2 eV is the Hartree energy, and $\epsilon_{xc} = \epsilon_x + \epsilon_c$ is the exchange-correlation energy.[39–41] $\epsilon_x = −(3/4)(3/2\pi)^{2/3}(1/r_s)$, and $\epsilon_c = −2A(1 + a_1 r_s)\ln[1 + 1/2\kappa A]$ are the exchange energy and the correlation energy respectively, for a uniform electron gas of density n, where $\kappa = b_1 r_s^{1/2} + b_2 r_s + b_3 r_s^{3/2} + b_4 r_s^{c+1}$, and A, c, a_1, b_1, b_2, b_3, and b_4 are constants obtained from.[39]

The probability $D(E_x)$ that an electron with longitudinal energy E_x (normal to the surface) can penetrate the potential barrier $\Phi(x)$ is given by the WKBJ approximation,[42]

$$D(E_x) = \exp\left[−\frac{2}{\hbar}\int_{x_1}^{x_2}\sqrt{2m_e[\Phi(x) − E_x]}dx\right], \quad (2)$$

where x_1 and x_2 are the two roots of $E_x − \Phi(x) = 0$, m_e is the electron rest mass. The tunneling current density from electrode 1 to the right, and from electrode 2 to the left, are respectively,[2,24,31]

$$J_1 = e\int_0^{\infty} N_1(E_x)D(E_x)dE_x, \quad (3a)$$

$$J_2 = e\int_0^{\infty} N_2(E_x)D(E_x)dE_x, \quad (3b)$$

$$N_1(E_x) = \frac{m_e k_B T}{2\pi^2\hbar^3}\ln\left(1 + e^{−(E_x−E_F)/k_B T}\right), \quad (3c)$$

$$N_2(E_x) = \frac{m_e k_B T}{2\pi^2\hbar^3}\ln\left(1 + e^{−(E_x + eV_g − E_F)/k_B T}\right), \quad (3d)$$

where $D(E_x)$ is given in Eq. (2), $N_{1,2}(E_x)dE_x$ is the total number of electrons inside electrode 1 (electrode 2) with longitudinal energy between E_x and $E_x + dE_x$ impinging on the surface of electrode 1 (2) across a unit area per unit time, calculated by the free-electron theory of metal,[43] m_e is the electron rest mass, $\hbar$ is the reduced Planck constant, k_B is the Boltzmann constant, and T is the electrode temperature.

Inside the insulator, $0 < x < D$, we solve the coupled Schrödinger equation and the Poisson equation, for the electric potential $eV(x)$

and the exchange-correlation potential $\Phi_{xc}(x)$,

$$-\frac{\hbar^2}{2m_e}\frac{d^2\psi}{dx^2} - [eV(x) - \Phi_{xc}(x)]\psi = E_0\psi, \tag{4}$$

$$\frac{d^2V(x)}{dx^2} = \frac{e\psi\psi^*}{\varepsilon_r\varepsilon_0}, \tag{5}$$

where ψ is the complex electron wave function, $n = \psi\psi^*$ is the electron density, and E_0 is the electron emission energy (with respect to the Fermi energy E_F). We assume $E_0 = 0$ in the calculation.

For a bias voltage V_g, the boundary conditions are, $V(0) = 0$, and $V(D) = V_g$. We also have the boundary conditions that both ψ and $d\psi/dx$ are continuous at $x = 0$, and $x = D$. Due to charge conservation, the net current density $J_{net} = J_1 - J_2 = e(i\hbar/2m_e)(\psi\psi^{*\prime} - \psi^*\psi')$ is constant for all x, where a prime denotes a derivative with respect to x, and $i = \sqrt{-1}$.

For convenience we use nondimensional quantities,[24] $\bar{x} = x/D$, $\phi = V(x)/V_g$, $\phi_{xc} = \Phi_{xc}/E_H$, $\phi_g = eV_g/E_H$, $\gamma = J/J_{CL}$, $\overline{E_0} = E_0/eV_g$, $\bar{n} = n/n_0 = \psi\psi^*/n_0$, $\lambda = D/\lambda_0$ where $\lambda_0 = \sqrt{\hbar^2/2em_eV_g}$, $J_{CL} = (4/9)\epsilon_0\sqrt{2e/m_e}V_g^{3/2}/D^2$ is the Child-Langmuir law,[44,45] $n_0 = (2\epsilon_0/3e)V_g/D^2$, and E_H is the Hartree energy. The wave function in the normalized form is $\psi(\bar{x}) = \sqrt{n_0}q(\bar{x})e^{i\theta(\bar{x})}$, where $q(\bar{x})$ and $\theta(\bar{x})$ are the nondimensional amplitude and phase respectively, both assumed real. Equations 4 and 5 are normalized to read,

$$\frac{d^2q}{d\bar{x}^2} + \lambda^2\left[\phi - \frac{\phi_{xc}}{\phi_g} - \frac{4}{9}\frac{\gamma_{net}^2}{q^4} + \overline{E_0}\right]q = 0, \tag{6}$$

$$\frac{d^2\phi}{d\bar{x}^2} = \frac{2}{3}\frac{q^2}{\varepsilon_r}, \tag{7}$$

where $\gamma_{net} = \gamma_1 - \gamma_2$ is the net normalized current density. The boundary conditions to eqs. (6) and (7) are, $\phi(0) = 0$, $\phi(1) = 1$,

$$q(1) = \left\{\left(\frac{2}{3\sqrt{1+\overline{E_0}}}\right)\left[\gamma_1 + \gamma_2 + 2\sqrt{\gamma_1\gamma_2}\cos\left(2\lambda\sqrt{1+\overline{E_0}}\right)\right]\right\}^{1/2},\text{ and}$$

$$q'(1) = \left(\frac{4}{3}\right)\left(\frac{\lambda\sqrt{\gamma_1\gamma_2}}{q(1)}\right)\sin\left(2\lambda\sqrt{1+\overline{E_0}}\right).$$ The normalized emission current density γ_1 and γ_2 are,

$$\gamma_1 = \frac{9}{4\pi\sqrt{2}}\frac{\lambda^2}{\phi_g^{5/2}}\overline{T}\int_0^\infty \ln\left(1 + e^{-\frac{\overline{E_x}-\overline{E_F}}{\overline{T}}}\right)D(\overline{E_x})d\overline{E_x}, \tag{8a}$$

$$\gamma_2 = \frac{9}{4\pi\sqrt{2}}\frac{\lambda^2}{\phi_g^{5/2}}\overline{T}\int_0^\infty \ln\left(1 + e^{-\frac{\overline{E_x}+\phi_g-\overline{E_F}}{\overline{T}}}\right)D(\overline{E_x})d\overline{E_x}, \tag{8b}$$

where $\overline{T} = k_BT/E_H$, $\overline{E_x} = E_x/E_H$, and $\overline{E_F} = E_F/E_H$. By solving eqs. (6) –(8) iteratively with the boundary conditions, we can self-consistently obtain the complete potential barrier profile $\Phi(x)$, the current density emitted from both electrodes J_1 and J_2, for any metal electrodes (W_1, W_2), insulator layer (ε_r, X, D), and bias voltage (V_g). It is found the tunneling current emission is insensitive to the temperature and the Fermi level.[24] In our calculations, we assume room temperature $T = 300$ K and $E_F = 5.53$ eV.

In this formulation, we have assumed, 1) the electron transmission probability during the emission process can be approximated by the WKBJ solution, where the metal electrodes are based on the free electron gas model; 2) the surfaces of the electrodes are flat and the problem is one-dimensional; 3) the image potential can be approximated by the classical image charge methods; and 4) the two metallic electrodes are separated by a sufficiently thin insulating film (in the nano- or subnano- meter scale), so that charge trapping in the insulator are ignored.[27,46]

III. RESULTS AND DISCUSSION

Figure 2a shows the normalized current density γ as a function of applied gap voltage V_g, for two electrodes having work functions, $W_1 = 4.1$ eV and $W_2 = 5.1$ eV (Au), separated by 1 nm
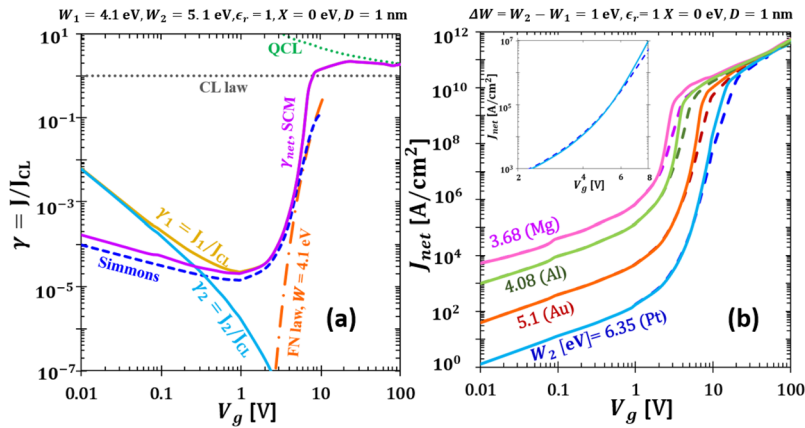

FIG. 2. (a) Normalized (in terms of CL law) current density γ as a function of applied gap voltage V_g, for two electrodes having work functions, $W_1 = 4.1$ eV and $W_2 = 5.1$ eV (Au), separated by 1 nm vacuum gap ($\varepsilon_r = 1$, $X = 0$ eV). Metal 2 is positively biased. The calculations are from SCM with both space charge and V_{xc} included. Simmons' formula (dashed line) is from Ref. 25, Fowler-Nordheim (FN) law (dash-dotted line) is from Refs. 47–49, calculated with the cathode work function $W = 4.1$ eV, and the quantum CL law (green dotted line) is from Refs. 29 and 30. (b) Current density J_{net} in A/cm^2 as a function of applied gap voltage V_g, for $D = 1$ nm and vacuum gap ($\varepsilon_r=1$, $X = 0$ eV). Solid and dashed lines in (b) represent RB and FB conditions respectively. Top to bottom, $W_2 = 3.68$ eV (Mg), 4.08 eV (Al), 5.1 eV (Au), 6.35 eV (Pt). The work function difference between the two metals is kept fixed, $\Delta W = W_2 - W_1 = 1$ eV. The inset in (b) represents the zoomed in view of the cross over behavior for the case of $W_2 = 6.35$ eV.

vacuum gap ($\epsilon_r = 1$, $X = 0$ eV). Metal 2 is given a positive bias (i.e. reverse bias, equivalent to Figs. 1a and 1c). The current densities are calculated from the SCM with both space charge potential and exchange correlation potential V_{xc} included. The $J - V$ curves may be roughly divided into three regimes: direct tunneling regime (V_g < 1V), field emission regime (1V < V_g < 10V), and space-charge-limited regime (V_g > 10V), similar to the MIM with electrodes of the same material.[24]

In the direct tunneling regime, just like similar MIM junctions,[24] the tunneling current density from cathode γ_1 and that from anode γ_2 are comparable. The net current density γ_{net} can be orders of magnitude lower than both γ_1 and γ_2. Therefore, in this regime, both anode emission and cathode emission need to be considered for an accurate estimation of the tunneling current in the dissimilar MIM junction. In the direct tunneling regime, γ_{net} increases linearly with V_g, which implies that the dissimilar electrode MIM junction behaves like an ohmic resister. The $J - V$ characteristic matches well with the Simmons' formula in the direct tunneling regime.[25] In the field emission regime, γ_2 is much smaller compared to γ_1, because the effective barrier height at the cathode is reduced by the bias voltage. The net current density γ_{net} is approaching the Fowler-Nordheim (FN) law[47–49] as V_g increases. However, in the field emission regime, Simmons' formula gives a more accurate fit to the self-consistent SCM result, which is due to the inclusion of anode screening in Simmons' formula. Simmons' formula breaks down around $V_g = 4$V. When the gap voltage reaches $V_g = 8$V, the effective barrier height is depressed by V_g below the Fermi level of the cathode (i.e. equivalent to Fig. 1c). In the SCL regime, when V_g reaches 100V, the cathode current and therefore the net current approaches the quantum CL law (QCL),[29,30] which gives the maximum current density that can be transported across a vacuum nano-gap for a given V_g and D, with quantum corrections. Note that current saturation in the SCL regime was observed in recent experiments when the nanogap was excited by very short THz pulses.[38]

Fig. 2b shows the net current density J_{net} in A/cm^2 as a function of applied gap voltage V_g, in dissimilar MIM junctions separated by a 1 nm wide vacuum gap for a fixed $\Delta W = W_2 - W_1 = 1$ eV. Solid and dashed lines are for reverse biased (RB) (i.e. higher work function metal is positively biased) and forward biased (FB) (i.e. higher work function metal is negatively biased) current densities, respectively. The tunneling current density of a dissimilar MIM junction is very sensitive to its apparent barrier height. Fig. 2b shows that, at low voltages ($eV_g < \Delta W$), the characteristics are almost identical for the FB and RB conditions. In the region of $\Delta W < eV_g < W_2 - X$, the FB current exceeds slightly. At a higher voltage, the FB and RB characteristics cross over. The inset of Fig. 2b shows the zoomed in view of this cross over behavior for the case of $W_2 = 6.35$ eV. It is shown in Fig. 2b, as W_2 (and therefore W_1) increases, the FB and RB characteristics intersect at increased values of V_g, which agrees with the results reported by Simmons, in 1960.[25] The underlying reason for this crossover behavior is, in the high voltage region, the electrons inside the cathode (i.e. relatively negatively biased electrode) would see a lower (higher) triangular barrier of height W_1 (W_2) in the RB (FB) condition (Figs. 1c and 1d). For ($W_2 - X$) < eV_g < 20 eV, the asymmetry between FB and RB characteristics becomes significant. The asymmetry between FB and RB characteristics remain insensitive to the value of W_1 or W_2, when the work function

difference ΔW is kept fixed. When V_g approaches 100 V, the net current density for both FB and RB conditions converges to the value of QCL, since the SCL current density depends only on V_g and D, but not on work function. The effect of the electron affinity X of the insulating thin film on $J - V$ characteristics would be similar, that is, increasing X would be equivalent to decreasing W_1 and W_2, provided the relative permittivity ϵ_r of the insulator and the insulator thickness are unchanged.

The effects of work function difference $\Delta W = W_2 - W_1$ on the $J - V$ characteristics of a MIM junction separated by a 1 nm wide vacuum gap, are shown in Fig. 3. The work function of metal 2 is kept fixed, $W_2 = 6.35$ eV (Pt). Solid and dashed lines represent the RB and FB conditions, respectively. Unlike the previous case of fixed ΔW in Fig. 2b, in the field emission regime, the asymmetry between FB and RB currents increases significantly as $|\Delta W|$ increases. Work function difference between the two metal electrodes in a dissimilar MIM junction influences the $J - V$ characteristics more profoundly than the individual work functions. The dotted line in Fig. 3 ($\Delta W = 0$) represents the similar MIM junction ($W_1 = W_2 = 6.35$eV) tunneling current density. The curves for J_{net} lie above and below the $\Delta W = 0$ reference, for $W_1 < 6.35$ eV and $W_1 > 6.35$ eV respectively.

Figure 4 shows the effects of gap width (or insulator thickness) D on the tunneling current density in dissimilar MIM junctions. In Fig. 4a, RB and FB tunneling current densities are plotted as functions of applied gap voltage V_g for $D = 0.5$ nm, 1 nm, 1.5 nm, 2 nm and 3 nm. In Fig. 4b, tunneling current densities are plotted as functions of D for different externally applied bias voltages V_g. For small gap width ($D = 0.5$ nm in Fig. 4a), the asymmetry between FB and RB current densities tend to disappear. However, when D is increased, the asymmetry increases significantly. The FB and RB characteristics tend to crossover at about the same voltage. However, this crossover voltage is not exactly the same for all D (c.f. Fig. 4b, $V_g = 5$V), as
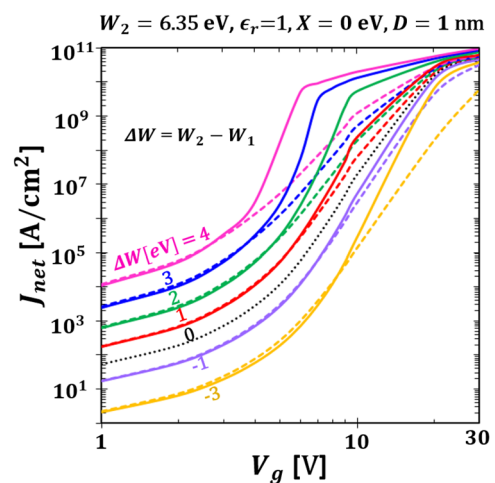

FIG. 3. The effects of work function difference ΔW on the $J - V$ characteristics of a dissimilar MIM junction with $D = 1$ nm, vacuum gap (ϵ_r=1, $X = 0$ eV). Top to bottom, $\Delta W = 4$ eV, 3 eV, 2 eV, 1 eV, 0 eV, -1 eV, -3 eV. The work function of metal 2 is kept fixed, $W_2 = 6.35$eV (Pt). Solid and dashed lines represent RB and FB conditions respectively.
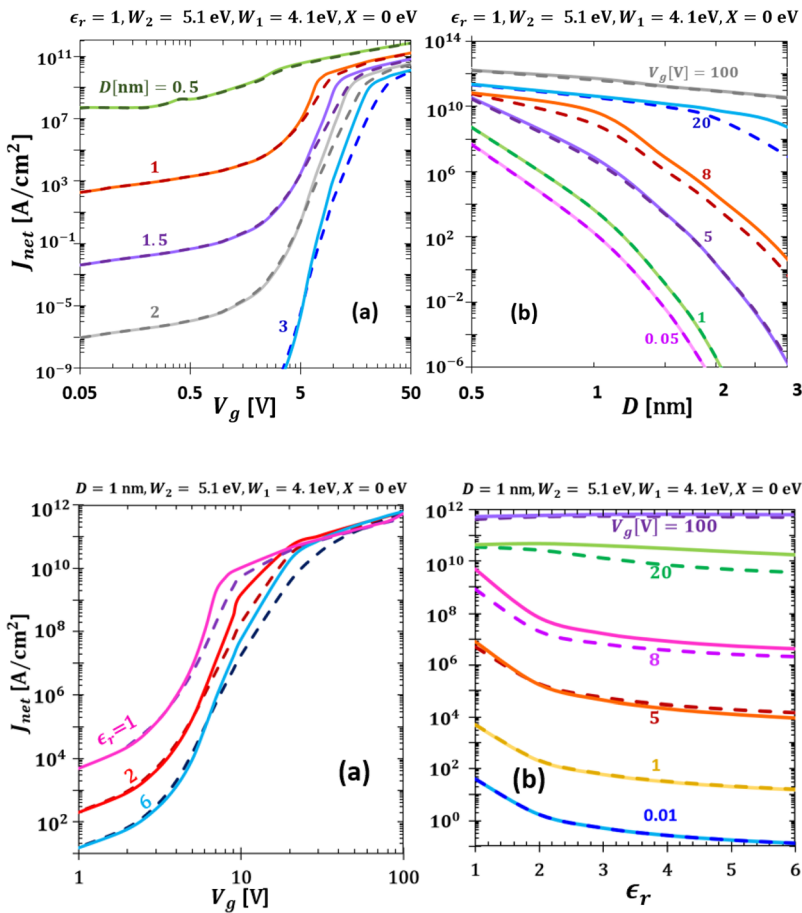
FIG. 4. The effects of gap width (D) on the $J - V$ characteristics of a dissimilar MIM junction with vacuum gap (a) J_{net} as a function of applied gap voltage V_g. Top to bottom, D = 0.5 nm, 1 nm, 1.5 nm, 2 nm, 3 nm. (b) J_{net} as a function of gap width D for different V_g. Work function of the two electrodes are W_2 = 5.1 eV and W_1 = 4.1 eV. For the vacuum gap ϵ_r = 1 and X = 0 eV. Solid and dashed lines represent RB and FB conditions respectively.

FIG. 5. The effects of relative permittivity of the insulating thin film ϵ_r on the $J - V$ characteristics of a dissimilar MIM junction with D = 1 nm. (a) J_{net} a function of applied gap voltage V_g. Top to bottom, ϵ_r = 1, 2 and 6 respectively. (b) J_{net} as a function of ϵ_r for different V_g. Work function of the two electrodes are W_2 = 5.1 eV and W_1 = 4.1 eV. Electron affinity of the insulator is X = 0 eV. Solid and dashed lines represent RB and FB conditions respectively.

previously reported by Simmons.[25] Figure 4b shows that the asymmetry between the FB and RB tunneling current densities appear only for high voltages. In low voltage regime ($V_g \leq 1$V for our MIM junction current calculations), for any given gap width (D = 0.5nm − 3nm), the current density profiles are almost identical for the two biases. The asymmetry increases with the applied bias voltage and it tends to disappear as V_g reaches 100V into the SCL regime. Note that, when D is large, the cathode emission current reaches the SCL current at a higher voltage. This explains the increase of asymmetry between FB and RB tunneling densities at high voltages (c.f. Fig. 4b, V_g = 20V) for large D.

Figure 5 shows the effects of insulator layer permittivity ϵ_r on the tunneling current density in dissimilar MIM junctions. In Fig. 5a, RB and FB tunneling current densities are plotted as functions of applied gap voltage V_g for ϵ_r = 1, 2 and 6. In Fig. 5b, tunneling current densities are plotted as functions of ϵ_r for different externally applied bias voltages V_g. The relative permittivity of insulating layer greatly influences the image charge potential as well as the space charge potential (Eq. 7), which in turn affect the current transport through the potential barrier. The asymmetry between FB and RB tunneling current densities increases with ϵ_r (Fig. 5a). However, for low voltages, there is no such asymmetry and the J_{net} profiles are identical, since in this direct tunneling regime the MIM junction

is ohmic (Figure 5b). The FB and RB characteristics crossover at higher voltages for increasing ϵ_r. It is important to note that, for low and intermediate bias voltages, J_{net} decreases with ϵ_r, but when V_g reaches 100V, this trend reverses because larger ϵ_r reduces the effect of space charge (Eq. 7). The asymmetry between FB and RB current densities tend to disappear as V_g reaches the quantum CL limit (Fig. 5a and Fig. 5b, V_g = 100V).

IV. CONCLUSIONS

Our self-consistent model characterizes the tunneling current in nano- and subnano-scale asymmetric (metal electrodes with dissimilar work functions) MIM junctions, taking into account the effects of both space charge and exchange-correlation potential. It provides accurate estimation of tunneling current density in different regimes over a wide range of input parameters. It is found that the Simmons' formulas provide good approximations of the tunneling current for only a limited parameter space in the direct tunneling regime. Their accuracy decreases when the effective barrier height decreases, where the self-consistent model would give a more accurate evaluation. We demonstrated the influences of electrode work functions (W_1 and W_2), insulator layer properties (ϵ_r, X), insulator thickness (D) and bias voltage (V_g) on the FB and RB tunneling

current density profiles. We found that the work function difference ΔW influences the asymmetry between forward and reverse bias $J - V$ characteristics more profoundly than their individual work functions. This asymmetry increases with increasing insulator layer thickness and relative permittivity. However, for very low (for our calculations, $V_g < 1V$) and very high voltages ($V_g \sim 100V$), the tunneling current density profiles are almost similar for the two biased cases.

It is worthwhile to note that, although the proposed model is developed for DC condition, it is applicable to the excitation of up to the Near Infrared frequency, since in typical metallic tunnel junctions, the tunneling events occur on a timescale much shorter than the period of the driving fields.[50] The effects of electrodes geometry, possible charge trapping inside the insulator film, frequency dependence will be subjects of future studies.

ACKNOWLEDGMENTS

REFERENCES

[1] J. C. Fisher and I. Giaever, J. Appl. Phys. **32**, 172 (1961).

[2] J. G. Simmons, J. Appl. Phys. **34**, 1793 (1963).

[3] S. Banerjee, J. Luginsland, and P. Zhang, Rev (2019).

[4] J. Tersoff and D. R. Hamann, Phys. Rev. B Condens. Matter **31**, 805 (1985).

[5] T. L. Cocker, V. Jelic, M. Gupta, S. J. Molesky, J. A. J. Burgess, G. D. L. Reyes, L. V. Titova, Y. Y. Tsui, M. R. Freeman, and F. A. Hegmann, Nat. Photonics **7**, 620 (2013).

[6] R. Esteban, A. G. Borisov, P. Nordlander, and J. Aizpurua, Nat. Commun. **3**, 825 (2012).

[7] K. J. Savage, M. M. Hawkeye, R. Esteban, A. G. Borisov, J. Aizpurua, and J. J. Baumberg, Nature **491**, 574 (2012).

[8] M. S. Tame, K. R. McEnery, S. K. Ozdemir, J. Lee, S. A. Maier, and M. S. Kim, Nat. Phys. **9**, 329 (2013).

[9] C. Li, E. T. Thostenson, and T.-W. Chou, Appl. Phys. Lett. **91**, 223114 (2007).

[10] W. S. Bao, S. A. Meguid, Z. H. Zhu, and G. J. Weng, J. Appl. Phys. **111**, 093726 (2012).

[11] N. Hu, Y. Karube, C. Yan, Z. Masuda, and H. Fukunaga, Acta Mater. **56**, 2929 (2008).

[12] P. Zhang, S. B. Fairchild, T. C. Back, and Y. Luo, AIP Adv. **7**, 125203 (2017).

[13] P. Zhang, J. Park, S. B. Fairchild, N. P. Lockwood, Y. Y. Lau, J. Ferguson, and T. Back, Appl. Sci. **8**, 1175 (2018).

[14] S. Vaziri, M. Belete, E. D. Litta, A. D. Smith, G. Lupina, M. C. Lemme, and M. Östling, Nanoscale **7**, 13096 (2015).

[15] V. Enaldiev, A. Bylinkin, and D. Svintsov, Phys. Rev. B **96**, 125437 (2017).

[16] F. Schwierz, *Two-Dimensional Electronics - Prospects and Challenges* (MDPI, 2018).

[17] M. Houssa, A. Dimoulas, and A. Molle, *2D Materials for Nanoelectronics* (CRC Press, 2016).

[18] P. Zhang and Y. Y. Lau, J. Plasma Phys. **82**, 595820505 (2016).

[19] P. Zhang, Á. Valfells, L. K. Ang, J. W. Luginsland, and Y. Y. Lau, Appl. Phys. Rev. **4**, 011304 (2017).

[20] J. Lin, P. Y. Wong, P. Yang, Y. Y. Lau, W. Tang, and P. Zhang, J. Appl. Phys. **121**, 244301 (2017).

[21] Y. Luo and P. Zhang, Phys. Rev. B **98**, 165442 (2018).

[22] D. J. Frank, R. H. Dennard, E. Nowak, P. M. Solomon, Y. Taur, and H.-S. Philip Wong, Proc. IEEE **89**, 259 (2001).

[23] A. Seabaugh, IEEE Spectr. Technol. Eng. Sci. News (2013).

[24] P. Zhang, Sci. Rep. **5**, 9826 (2015).

[25] J. G. Simmons, J. Appl. Phys. **34**, 2581 (1963).

[26] J. G. Simmons, J. Appl. Phys. **35**, 2472 (1964).

[27] R. I. Frank and J. G. Simmons, J. Appl. Phys. **38**, 832 (1967).

[28] J. G. Simmons, J. Phys. Appl. Phys. **4**, 613 (1971).

[29] Y. Y. Lau, D. Chernin, D. G. Colombant, and P.-T. Ho, Phys. Rev. Lett. **66**, 1446 (1991).

[30] L. K. Ang, T. J. T. Kwan, and Y. Y. Lau, Phys. Rev. Lett. **91**, 208303 (2003).

[31] L. Wu, H. Duan, P. Bai, M. Bosman, J. K. W. Yang, and E. Li, ACS Nano **7**, 707 (2013).

[32] L. K. Ang and P. Zhang, Phys. Rev. Lett. **98**, 164802 (2007).

[33] A. Singh, FIU Electron (Theses Diss, 2016).

[34] S. Krishnan, S. Bhansali, E. Stefanakos, and Y. Goswami, Procedia Chem. **1**, 409 (2009).

[35] K. Choi, F. Yesilkoy, G. Ryu, S. H. Cho, N. Goldsman, M. Dagenais, and M. Peckerar, IEEE Trans. Electron Devices **58**, 3519 (2011).

[36] W. Weinreich, R. Reiche, M. Lemberger, G. Jegert, J. Müller, L. Wilde, S. Teichert, J. Heitmann, E. Erben, L. Oberbeck, U. Schröder, A. J. Bauer, and H. Ryssel, Microelectron. Eng. **86**, 1826 (2009).

[37] J. Singh and B. Raj, Appl. Phys. A **125**, 203 (2019).

[38] K. Yoshioka, I. Katayama, Y. Minami, M. Kitajima, S. Yoshida, H. Shigekawa, and J. Takeda, Nat. Photonics **10**, 762 (2016).

[39] J. P. Perdew and Y. Wang, Phys. Rev. B **45**, 13244 (1992).

[40] W. Kohn and L. J. Sham, Phys. Rev. **140**, A1133 (1965).

[41] P. A. M. Dirac, Math. Proc. Camb. Philos. Soc. **26**, 376 (1930).

[42] D. Bohm, *Quantum Theory* (1951).

[43] M. A. Omar, *Elementary Solid State Physics. Principles And Applications*. compressed (2016).

[44] C. D. Child, Phys. Rev. Ser. I **32**, 492 (1911).

[45] I. Langmuir, Phys. Rev. **2**, 450 (1913).

[46] A. Rose, Phys. Rev. **97**, 1538 (1955).

[47] E. L. Murphy and R. H. Good, Phys. Rev. **102**, 1464 (1956).

[48] R. H. Fowler and L. Nordheim, Proc. R. Soc. A **119**, 173 (1928).

[49] K. L. Jensen and M. Cahay, Appl. Phys. Lett. **88**, 154105 (2006).

[50] P. Février and J. Gabelli, Nat. Commun. **9**, 4940 (2018).